Stress and Buckling of Internally Pressurized, Elastic-Plastic Torispherical Vessel Heads—Comparisons of Test and Theory

D. BUSHNELL

Lockheed Palo Alto Research Laboratory, Palo Alto, California

G. D. GALLETLY

Department of Mechanical Engineering, The University of Liverpool, England

Several aluminum and mild steel torispherical heads were tested by Galletly and by Kirk and Gill and subsequently analyzed by Bushnell with use of the BOSOR5 computer program. The thinnest specimens buckled at pressures for which part of the toroidal knuckle was stressed well beyond the yield point. The analysis includes large deflection effects, nonlinear material behavior, and meridional variation of the thickness. The calculated strains in the thicker specimens agree reasonably well with the test results, but the calculated prebuckling strains in the thinnest specimens are generally greater than the values measured in the torodial knuckle after the onset of plastic flow. Reasonably good agreement between test and theory is obtained for the buckling pressures of aluminum specimens, but the calculated buckling pressures for mild steel specimens are much lower than the observed values, a discrepancy that is attributed to circumferentially varying thickness and possible inability of the analytical model of the elastic-plastic material to predict accurately the state of stress in the toroidal knuckle where loading is nonproportional once yielding has occurred.

Introduction

Interest in internally pressurized torispherical heads was stimulated by the failure of a large fluid coker undergoing a hydrostatic proof test at Avon, California, in 1956. Galletly [1, 2][1] determined from an elastic, small-deflection analysis that the stresses exceeded the yield point of the material by considerable margins over substantial portions of the vessel. Galletly's work [1] stimulated Drucker and Shield [3, 4] to perform limit analyses of shells of revolution using simplified yield surfaces for a Tresca material. Other elastic-plastic analyses of torispherical shells were published by Gerdeen and Hutula [5], Crisp and Townley [6], and Simonen and Hunter [7]. Calladine [8] presented a novel analysis of the limit pressure of torispherical heads which gives results similar to those obtained by Shield and Drucker [4]. Save [9] conducted a series of tests on torispherical, toriconical, and flat heads. Several papers on the elastic-plastic analysis of pressure vessel heads may be found in [10], including contributions by Gerdeen [11], Mescall [12], and Marcal [13]. Other references to work in this area are given by Esztergar [14].

The possibility of nonaxisymmetric buckling of internally pressurized torispherical heads was first predicted by Galletly [2]. Fino and Schneider [15] reported such buckling in a head designed according to the ASME Code, but at a pressure slightly below the design pressure. It is likely that the unexpectedly low buckling pressure resulted from nonaxisymmetric imperfections generated when spherical and toroidal gores were welded together to form the very large head. Mescall [16] was the first to present a solution to the nonaxisymmetric stability analysis. He used elastic small deflection theory. Adachi and Benicek [17] conducted a series of buckling tests on torispherical heads made of polyvinyl chloride (PVC), chosen primarily because of the high yield stress to Young's modulus ratio, which ensures that buckling occurs before large-scale yielding. The correlation of elastic analysis with these tests was much improved by inclusion of nonlinear geometrical effects. Thurston and Holston [18] were the first to take account of moderately large axisymmetric prebuckling meridional rotations in the stability analysis of these heads. Since publication of [18] many computer programs have been written which will calculate nonsymmetric buckling loads of arbitrary elastic shells of revolution including geometric nonlinearity in the prebuckling analysis and prebuckling shape changes in the stability analysis [19-23].

Recently two papers have appeared on nonsymmetric buckling of elastic-plastic shells: Brown and Kraus [24] calculated critical

[1] Numbers in brackets designate References at end of paper.

Contributed by the Pressure Vessels and Piping Division and presented at the Petroleum Mechanical Engineering and Pressure Vessels and Piping Conference, Mexico City, Mexico, September 19–24, 1976, of THE AMERICAN SOCIETY OF MECHANICAL ENGINEERS. Manuscript received at ASME Headquarters, May 24, 1976. Paper No. 76-PVP-23.

pressures for internally pressurized ellipsoidal heads with use of small deflection theory, and Bushnell and Galletly [25] found buckling loads for externally pressurized torispherical heads pierced by nozzles and for conical heads with use of large deflection theory in the prebuckling analysis.

The purpose of this paper is to present comparisons between test and theory for internally pressurized torispherical heads tested by Kirk and Gill [26] at the University of Manchester Institute of Science and Technology and by Galletly [27] at the University of Liverpool in England. All torispherical heads were joined to cylindrical segments long enough to eliminate the effect of clamping at the base of the cylinder on stresses and buckling modes in the toroidal knuckle. The analysis was performed with use of the BOSOR5 computer program [28].

Tests by Kirk and Gill and by Galletly

The test specimens, material properties, and test rig and instrumentation for Kirk and Gill's tests are shown in [26] and for Galletly's tests are shown in [27]. Table 1 gives the stress-strain data as used in BOSOR5. Table 2 lists the nominal dimensions of the specimens treated in this paper. These dimensions are identified in Fig. 1. Variations of thickness along the meridians of the thinnest of Kirk and Gill's specimens are listed in Table 3. These thickness distributions correspond to the meridians at which the first buckle appeared. Variations of the thickness around the circumference are plotted in Fig. 2. These circumferential variations correspond approximately to the meridional stations at which the buckling modal displacements were maximum. The percentage variation in thickness along each meridian is greater than the variation around the circumference. Imperfections of the meridian contours were determined in Kirk and Gill's specimens with a Ferranti 3-axis measurement machine that had a resolution of 0.0025 mm. Fig. 3 shows the initial imperfections along the worst meridian for each of the thinnest specimens. Circumferential variations in thickness and meridional and circumferential deviations from the nominal meridional shape are neglected in the analysis presented here.

In the Galletly tests strain gages were glued to two of the mild steel specimens only, MS3 and MS4. Specimen MS3 was of better geometrical quality than MS4, and therefore more strain gages were affixed to it. The gages were attached at locations where the first buckles were expected to appear. Strips of ten gages each were attached to meridians at circumferential coordinates $\theta = 118$ deg and 214 deg, both on the outside and on the inside surfaces of the specimen. Half of these gages measured circumferential strains and half measured meridional strains. Also, two meridional strips of six double gages each were attached to the outside and inside of MS3 at $\theta = 86$ deg. All three meridional strips were to measure outer and inner fiber

Table 1 Stress-strain data used in the BOSOR5 analysis[a]

Galletly's specimens				Kirk & Gill's specimens	
Aluminum $E = 70{,}864$ MN/m² $\nu = 0.32$		Mild steel $E = 206{,}400$ MN/m² $\nu = 0.3$		Aluminum $E = 70{,}122$ MN/m² $\nu = 0.32$	
Stress $(\sigma/E) \times 10^2$	Strain (%)	Stress $(\sigma/E) + 10^2$	Strain (%)	Stress $(\sigma/E) \times 10^2$	Strain (%)
0.400	0.40	0.1180	0.118	0.271	0.271
0.4369	0.45	0.1200	1.30	0.298	0.303
0.4675	0.50	0.1267	1.50	0.317	0.350
0.4913	0.55	0.1333	1.80	0.327	0.40
0.5058	0.60			0.338	0.47
0.5121	0.65			0.345	0.60
0.5145	0.70			0.354	0.80
0.5243	0.90			0.361	1.60
0.5243	1.00				

[a] In BOSOR5 the actual stress-strain curve is represented as a series of straight segments joined at the points given here.

Table 2 Internally pressurized torispherical heads

Specimen	Tested By	Mat'l[a]	Geometry					Buckling Test Results $(p_{cr}/E) \times 10^6$	BOSOR 5 Buckling Predictions			
			t_n (mm)	R_c/t_n	R_t/t_n	R_s/t_n	L_c/R_c		Elastic-Plastic		Elastic	
									Flow Theory	Deformation Theory	Linear	Nonlinear
A1	Galletly	Aluminum	0.127	540	220	1080	0.6	8.25	8.93 (45)[b]	8.93 (45)	5.7 (50)	13.7 (50)
A2	Galletly	Aluminum	0.254	270	110	540	0.6	20.87	21.36 (21)	20.90 (25)		
A3	Galletly	Aluminum	0.254	270	110	540	0.6	21.84	22.91 (25)	21.34 (29)	24.0 (37)	No buckling
MS1	Galletly	Mild Steel	0.127	540	220	1080	0.6	4.23	1.47 (30-40)		4.0 (55)	6.9 (55)
MS2	Galletly	Mild Steel	0.127	540	220	1080	0.6	2.60	1.17 (30-40)		1.67 (65)	4.3 (55)
MS3	Galletly	Mild Steel	0.127	540	220	1080	0.6	2.73	2.00 (27)	1.73 (27)	5.01 (50)	10.77 (50)
MS4	Galletly	Mild Steel	0.127	540	220	1080	0.6	2.50	1.77 (28)		3.4 (55)	8.3 (50)
4A	Kirk & Gill	Aluminum	0.254	266	40	531	1.0	3.44 (75)	5.13 (40)	4.28 (35)	11.4 (75)	15.3 (65)
4B	Kirk & Gill	Aluminum	0.254	266	60	531	1.0	5.40 (62)	6.85 (40)	5.70 (35)	12.8 (60)	19.7 (50)
4C	Kirk & Gill	Aluminum	0.254	266	90	531	1.0	10.81 (49)	10.48 (28)	9.41 (40)	14.3 (45)	34.8 (45)
1C	Kirk & Gill	Aluminum	2.54	26.6	9	53.1	1.0	–	–	–	–	–
3A	Kirk & Gill	Aluminum	0.635	106	16	212	1.0	–	–	–	–	–
3B	Kirk & Gill	Aluminum	0.635	106	24	212	1.0	–	–	–	–	–
3C	Kirk & Gill	Aluminum	0.635	106	36	212	1.0	–	–	–	–	–

(a) Stress-strain curves are given in Table 1.
(b) Numbers in parentheses are circumferential waves in the buckling mode.

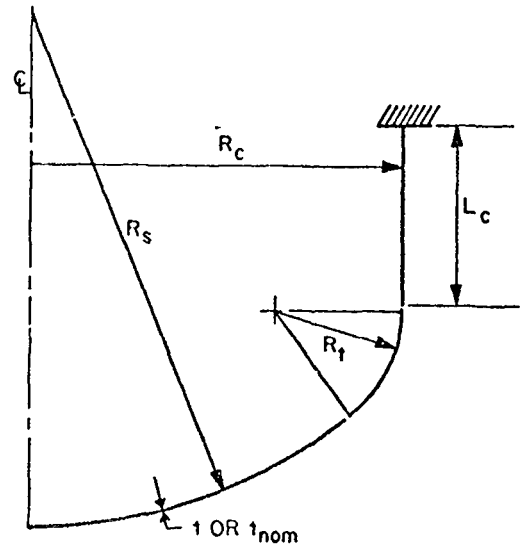

Fig. 1 Geometry of torispherical shells tested by Kirk and Gill and by Galletly

circumferential and meridional strains in the neighborhood of the juncture between the spherical and the toroidal segments. In addition, two series of 22 gages each for measuring external and internal circumferential strains were attached at 6-1/2-deg intervals in the ranges 86 deg $\leq \theta \leq$ 158 deg and 173 deg $\leq \theta \leq$ 246 deg. This circumferential band was located at an axial distance z = 13.7 mm from the crown. The preliminary buckling analysis had led to a prediction that nonsymmetric buckling modal displacements would be maximum near this location, which is in the toroidal knuckle quite close to the juncture between the knuckle and the spherical segment. All gages were attached opposite each other on inside and outside surfaces of the shell wall. It was hoped that this arrangement of gages would lead to early detection of circumferential buckles before they became visible.

Fewer gages were attached to specimen MS4, and they were not affixed at opposite internal and external locations.

All gages were the Micro-Measurement type: The strips of ten gages along meridians were Type EA-06-031 MH-120; the circumferential bands of gages to measure hoop strains were Type EA-06-062 AA-120; and the meridional strip of six double gages at θ = 86 deg in specimen MS3 were Type EA-06-062 TT-120.

Analysis

Details of the analysis method are given in [29–31] and a summary is presented in the companion paper to this [32]. The BOSOR5 computer program [28] was used for the calculations. This program is applicable to any segmented or branched, ring-stiffened shell of revolution.

Axisymmetric Prebuckling Analysis. In the axisymmetric prebuckling analysis, large deflection effects and elastic-plastic material behavior are simultaneously accounted for by means of a double iteration loop. In the inner loop the nonlinear equations including terms due to moderately large deflections are solved by the Newton method. Material properties are held constant in this loop. In the outer loop the material properties are updated by means of a subincremental process described in detail in [29]. This subincremental process permits the use of rather large load increments without excessive loss of accuracy in the solution. Plasticity calculations are based on the von Mises yield criterion and associated flow rule with isotropic strain hardening. Incremental flow theory is always used for the prebuckling analysis. Iterations over the inner and outer loops continue at a given load level until the displacement vector converges within a certain prescribed amount. In this way the favorable convergence property of the Newton procedure is preserved, equilibrium is satisfied within the degree of approximation inherent in a discrete model, and the flow law of the material is satisfied at every point in the structure at every load increment. The effect of the rotation of the surface on the work done by the pressure during deformation is included in the analysis.

Nonsymmetric Buckling Analysis. Bifurcation buckling loads corresponding to nonsymmetric buckling modes are calculated in the following way: The user of BOSOR5 first selects an initial number of circumferential waves n_o which he feels corresponds to the minimum bifurcation load. For this wave number n_o the stability determinant is calculated for each load increment. The load is increased until the stability determinant changes sign or until eigenvalues are detected between two sequential load steps or until the maximum allowable user-specified load has been reached. At this point in the calculations a series of eigenvalue problems of the form

Table 3 Internally pressurized torispherical shells tested by Kirk and Gill. Thickness versus arc lengths in segments used in the BOSOR5 analysis (nominal thickness t_n = 0.254 mm)

	Specimen 4A		Specimen 4B		Specimen 4C	
	s(mm)	t/t_n	s(mm)	t/t_n	s(mm)	t/t_n
Segment #1 Spherical	0	1.00	0	0.87	0	1.04
	18.16	1.00	27.1	0.87	27.1	1.04
	38.08	1.05	43.36	0.95	55.271185	1.01
	52.17	1.06	54.2	0.91		
	57.99	0.95		0.93		
	64.424	0.89				
Segment #2 Toroidal knuckle	0.0	0.89	0.0	0.93	0	1.01
	3.596	0.85	5.434	0.90	4.6188	0.88
	7.666	0.93	9.499	0.91	12.8853	1.00
	11.111	0.98	13.5639	0.80	18.9828	0.79
			17.05711	1.04	23.0478	0.94
					26.54915	1.37
						1.06
Segment #3 Cylinder	0.0	0.98	0.0	1.04	0	1.06
	15.0	1.07	15.0	1.05	15.0	1.02

$$[A(n) + \lambda_n B(n)]x_n = 0 \quad (1)$$

is set up, where

- $A(n)$ = the stiffness matrix corresponding to n circumferential waves of the structure as loaded by L_1 (see following definitions)
- $B(n)$ = the load-geometric matrix corresponding to the prestress increment resulting from the load increment $L_2 - L_1$
- L_1 = the load state just before the sign change of the stability determinant
- L_2 = the load state just after the sign change of the stability determinant
- λ_n = the eigenvalue
- x_n = the eigenvector
- n = the number of circumferential waves lying in a range $n_{\min} \leq n \leq n_{\max}$, with $n_{\min}$ and $n_{\max}$ provided by the program user—note that the initial guess n_o also lies in the range $n_{\min} \leq n_o \leq n_{\max}$

BOSOR5 computes a series of eigenvalues λ_n and eigenvectors x_n for $n_{\min} \leq n \leq n_{\max}$ in wave number increments of n_{incr}, which is also supplied by the program user. In most cases (but not all!) the minimum λ_n corresponds to the critical bifurcation buckling load. It sometimes happens that as the load increases the prestress in the shell decreases. (See Fig. 25, for example.) If this phenomenon occurs in the load range for which the stability determinant first vanishes, as is often the case for internally pressurized vessel heads of the type being considered here, the critical wave number corresponds to that in which $|\lambda_n|$ rather than λ_n is minimum. More details on the bifurcation buckling analysis appear in [30–32].

The program user may select either the incremental flow theory or the deformation theory as a basis for calculating the stability determinant. These two options were programmed into BOSOR5 because buckling loads obtained with use of deformation theory are often in better agreement with test results than are those obtained with use of flow theory. The reasons for this anomaly are not yet well understood, but it is clear that the post-yield biaxial hardening and flow laws are involved.

Comparison With Tests by Adachi and Benicek [17]. In order to check the adequacy of BOSOR5 for prediction of buckling of internally pressurized torispherical shells, the elastic PVC specimens tested by Adachi and Benicek [17] were analyzed. The results from test and theory are shown in Fig. 4. The curves for the test results are generated from an empirical formula derived by Adachi and Benicek:

$$10^6 p/E = C[10^3 t/R_i]^m \quad (2)$$

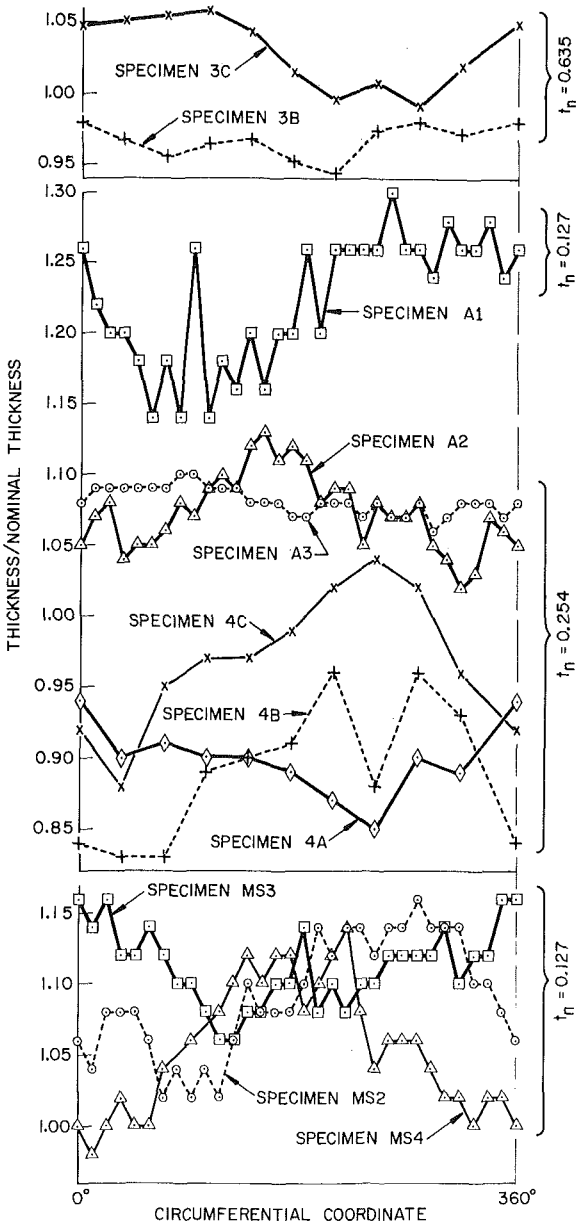

Fig. 2 Measured thickness around the circumference at the latitudes where the maximum normal buckling modal displacement is predicted to occur

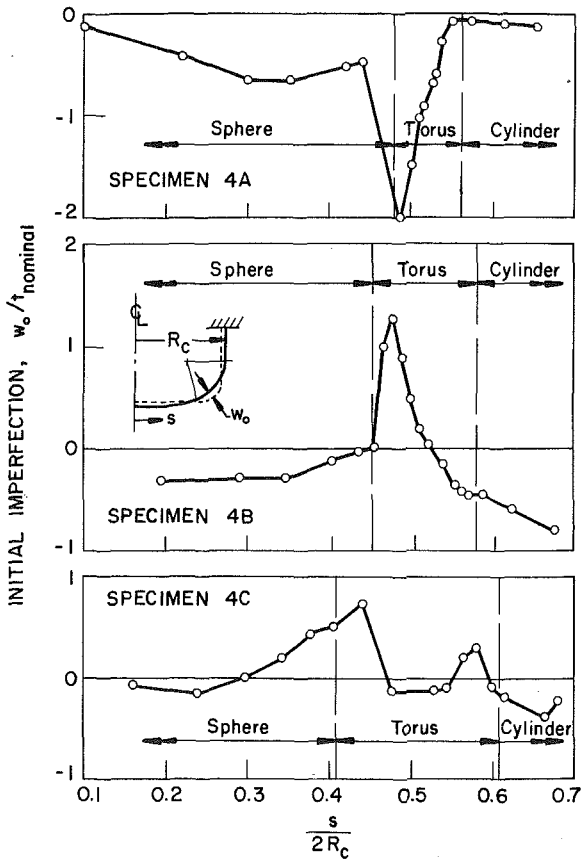

Fig. 3 Initial imperfections of the meridional contours of the thinnest Kirk and Gill specimens. These imperfections are not accounted for in the BOSOR 5 analysis.

in which C and m depend on the juncture angle ϕ and the ratio of the toroidal knuckle radius R_t to the cylinder diameter $2R_c$. Good agreement was obtained between test and theory. Therefore the decision was made to proceed with the inelastic stress and buckling analyses of the Kirk and Gill and of the Galletly specimens.

Prebuckling Behavior

Comparison of Test and Theory for Kirk and Gill's Specimens. All of the specimens were analyzed with the discrete models such as shown in Fig. 5. (The cylindrical segment has been truncated in Fig. 5 in order to save space. It was clamped.) Preliminary convergence studies demonstrated that 30 nodal points were adequate for treatment of the knuckle region and that Simpson's rule of numerical integration through the wall thickness could be performed sufficiently accurately with use of five points through the thickness. All specimens were analyzed with use of the stress-strain data given in Table 1. Specimens 1C, 3A, 3B, and 3C were assumed to be of constant thickness. The thickness variations for specimens 4A, 4B, and 4C are given in Table 3. The reference surface was taken as the inner surface, and its geometry is given in Table 2. All shells are assumed to be axisymmetric.

Fig. 6 shows the predicted and experimentally measured normal displacement at two points on specimen 3B: at the apex where the displacement is maximum outward and in the middle of the toroidal knuckle where the displacement is maximum inward. Notice that BOSOR5 overestimates the inward deformation of the knuckle at higher pressures. This discrepancy consistently occurs for all of the specimens analyzed. Possibly it arises from the slight anisotropy of the material from which the specimens were machined. Fig. 7 shows the distribution of normal displacement at the highest pressure for which strain gage readings were available.

Figs. 8 and 9 show strain distributions at various pressures for specimens 3A, 3B, 3C, and 4C, and Fig. 10 shows the maximum external and internal strains as functions of pressure. Except for specimen 3A, the agreement between test and theory is better in the elastic range than in the plastic range and better for the thicker specimens 3A, 3B, 3C than for the thinner one, 4C. BOSOR5 tends to overestimate strains in the plastic range. Again, this discrepancy may be due to material anisotropy not accounted for in the analysis, or it may be due to imperfections in specimen geometry which tend to affect the plastic behavior more than the

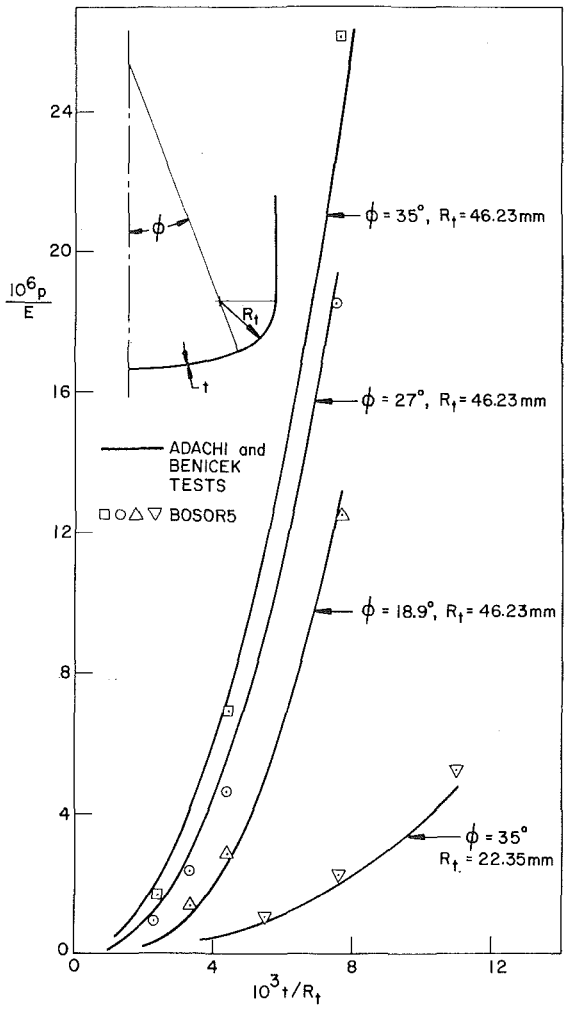

Fig. 4 Comparison of experimental and theoretical bifurcation buckling pressures for the elastic polyvinyl chloride (PVC) specimens tested by Adachi and Benicek

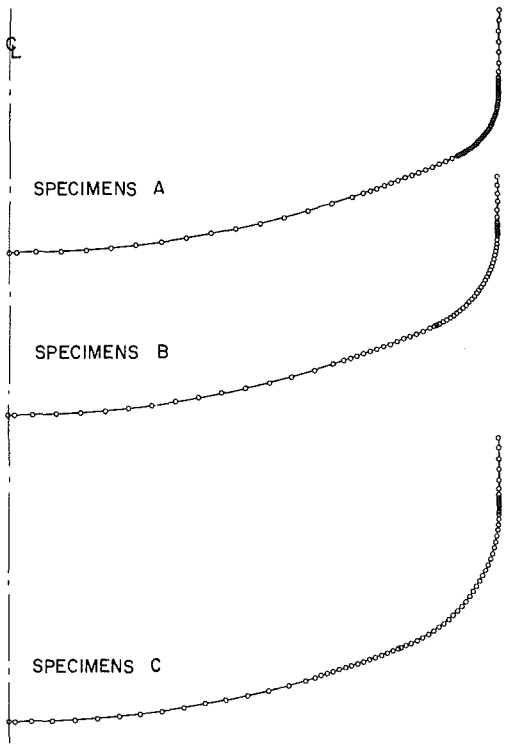

Fig. 5 Discrete models for analysis by BOSOR5

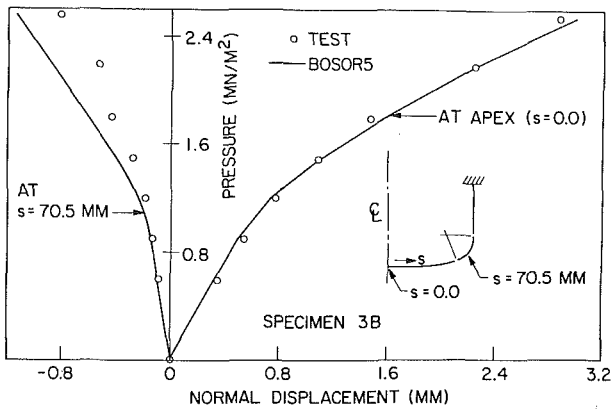

Fig. 6 Maximum outward and inward normal displacements measured by Kirk and Gill and calculated by BOSOR5 for specimen 3B

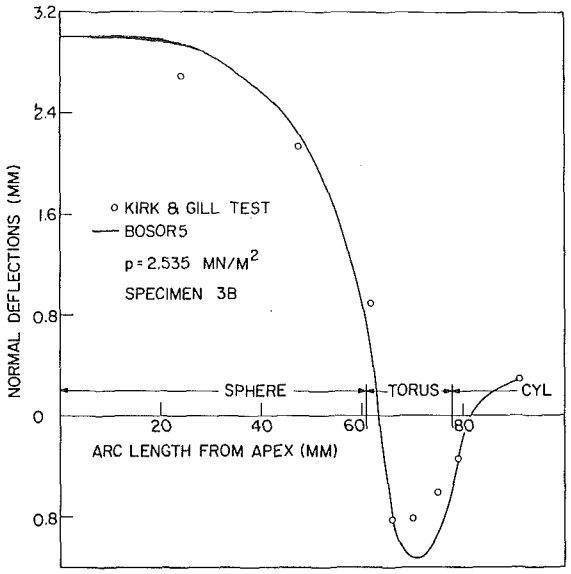

Fig. 7 Measured and calculated normal displacement distribution at a high pressure

elastic behavior, or it may result from the inadequacy of the isotropic strain hardening material model to predict accurately the biaxial plastic flow in the toroidal knuckle region-flow which deviates considerably from proportional loading as the effective stress increases beyond the proportional limit of the aluminum.

Fig. 11 shows hoop strain as a function of pressure in specimen 1C, one of the thickest specimens tested by Kirk and Gill. The agreement between test and theory is reasonably good.

Strain of Galletly's Mild Steel Specimen MS3. Specimen MS3 was the only vessel tested by Galletly that had circumferential and meridional strain gages affixed opposite one another on the inside and outside surfaces. Figs. 12–15 show some of the test results and comparisons with BOSOR5 calculations. In this case and for the other mild steel specimens, it was necessary to use a minimum of 40 nodal points in the toroidal knuckle because the shell was only half as thick as the thinnest of Kirk and Gill's specimens. If fewer nodes are used, the predicted strain distribution in the region near the sphere-torus juncture becomes jagged and the strains in the knuckle away from this juncture are grossly overestimated. In general, with use of BOSOR5 for the treatment of very thin torispherical heads ($R_c/t > 250$), it is advisable for the analyst to use from 60 to 90 nodes in each of the spherical and toroidal segments. Fewer nodes were used in the present analysis because a convergence study had first been undertaken in order to determine an adequate discrete model. The thickness distribution used in the analysis is given in Table 4. Thicknesses are assumed to vary linearly between stations where they are specified. Again, circumferential varia-

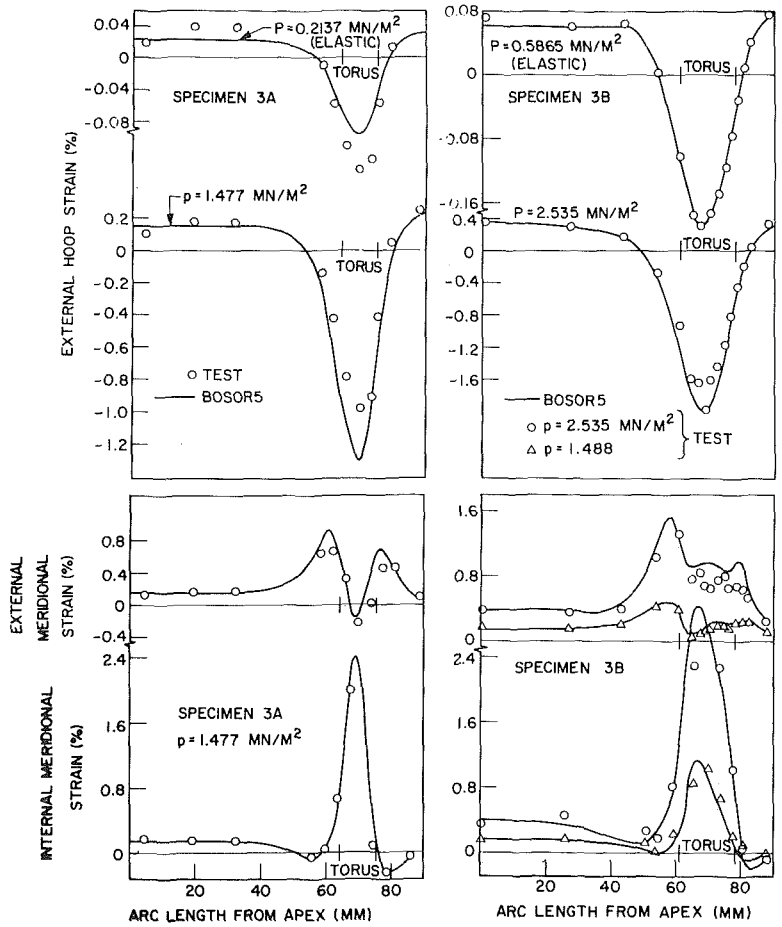

Fig. 8 Comparison of test and theory for strain distributions in specimens 3A and 3B

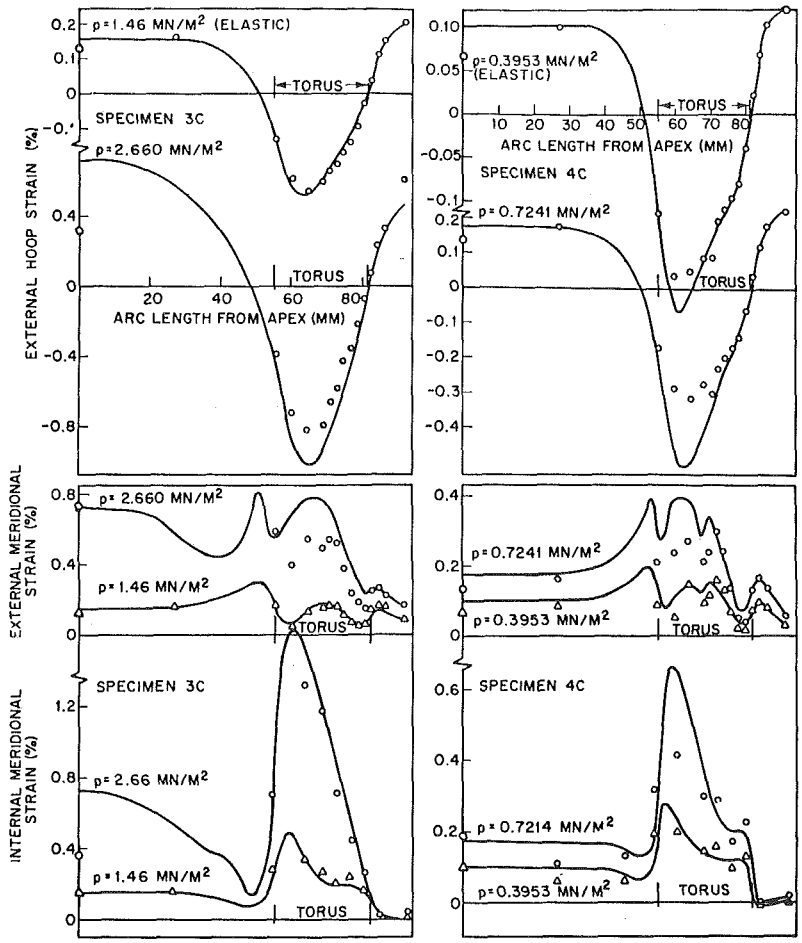

Fig. 9 Comparisons of test and theory for strain distributions in specimens 3C and 4C

tion of the thickness is not accounted for in the BOSOR5 analysis.

Figs. 12–14 show the measured growth of circumferential membrane and bending strains with increasing pressure. Two facts emerge from these figures. Fig. 12 shows that BOSOR5 predicts much higher average circumferential membrane strains than those indicated in the test as the material is stressed above the yield point, and Figs. 13 and 14 show that the deformations in the torodial knuckle at $z = 13.7$ mm are not axisymmetric. It seems probable that the gradual growth of circumferential waves, so evident from the test results plotted in Figs. 13 and 14, tends to relieve the hoop membrane strain that apparently would grow more rapidly if the knuckle were perfectly axisymmetric.

Fig. 15 shows the average hoop strain and internal meridional strain at certain axial locations on specimen MS3. The dashed curve labeled "STAGS" was obtained with a computer program of that name written by Almroth, Brogan, and Stanley [33] for the analysis of general elastic-plastic shells. In the STAGS discrete model, only 15 nodes were located in the toroidal knuckle. It is porbable that a STAGS run with use of more degrees of freedom would bring the two theoretical results for the meridional strain at $z = 11.2$ mm into better agreement. This strain component varies more steeply in the knuckle than does the hoop strain, and therefore more nodal points must be used in order to predict its distribution with the same degree of accuracy.

Notice that the rather gross disagreement between test and theory for this specimen pressurized above the elastic limit is similar to the discrepancy found in the case of the thinnest of Kirk and Gill's specimens, 4C, for which a similar plot is given at the top of Fig. 10. It seems likely, therefore, that considerable prebuckling circumferential bending occurred in Kirk and Gill's thinnest specimens also, since the variation of thickness around the circumference of specimen 4C was similar in nature and magnitude to the circumferential nonuniformity of Galletly's specimen MS3, as seen in Fig. 2. This nonsymmetric behavior of the very thin test specimens is probably the major cause of the disagreement between test and theory in the prediction of the prebuckling state of strain above the elastic limit.

Nonsymmetric Buckling

Description of the Postbuckling Phenomenon. Adachi and Benicek [17] first described the postbuckling phenomenon of internally pressurized torispherical shells. At some pressure, called the critical pressure, a single buckle appears somewhere on the circumference in the toroidal knuckle. This buckle has a very short wavelength in the circumferential direction but covers most of the meridional arc of the knuckle. If the first buckle does not cause fracture, the pressure can be further increased. Other isolated buckles then appear, usually one or two at a time, spaced far apart on the circumference compared to their circumferential wavelengths. It is probable that each buckle causes the circumferential compressive stress in the knuckle to be somewhat relieved for a considerable circumferential arc. This would explain why the buckles are isolated.

The postbuckling phenomenon observed by Kirk and Gill and by Galletly is similar. The buckles in Adachi and Benicek's elastic PVC specimens were inward and those in the elastic-plastic

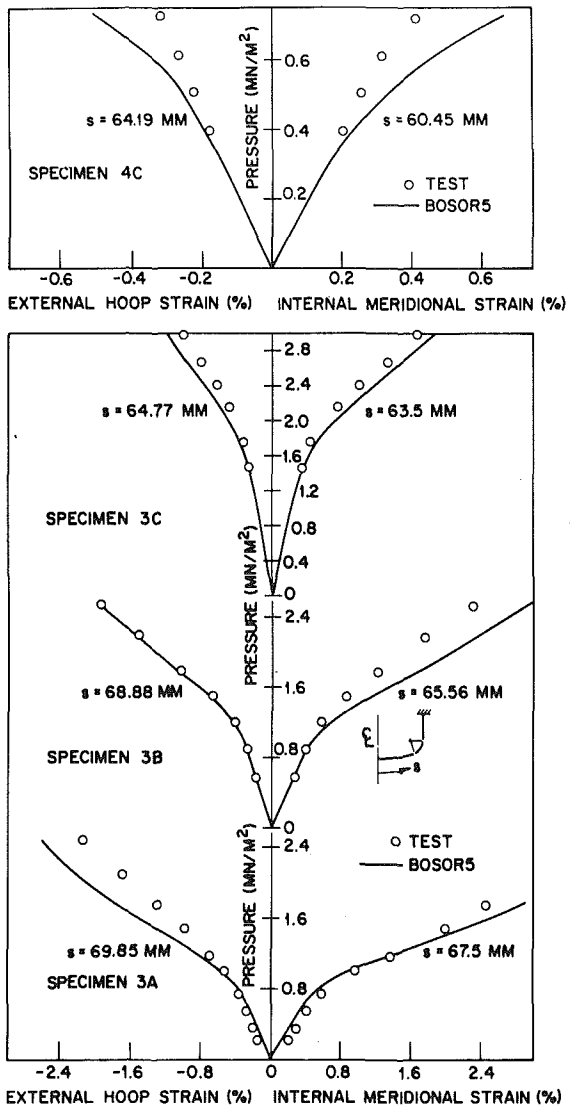

Fig. 10 Comparison of test and theory for the maximum external and internal strains in specimens 3A, 3B, 3C, and 4C

metallic specimens appear at first to be generally outward. Figs. 16 and 17 show some of the specimens after test. Table 5 lists the pressures at which buckles appeared and their circumferential locations. Fig. 18 shows the plots generated by Kirk and Gill's rotating displacement transducer. The tiny wiggles are the incipient buckles, not visible to the unaided eye. For example, the first incipient buckles in specimen 4B were detected at a dimensionless pressure $10^6\, p/E$ of about 5.40. The circumferential wavelength of each incipient buckle was approximately 6.7 mm. About 60 such buckles could fit around the circumference if they occurred as a continuous sine wave.

As the pressure is increased, the isolated incipient buckles, not visible at first, grow until suddenly they become visible. The dimensionless critical pressures listed in Table 2 for Kirk and Gill's specimens 4A, 4B, and 4C are the pressures at which the incipient buckles were first detected by the rotating transducer. The dimensionless critical pressures for Galletly's specimens are those at which the buckles first became visible to the unaided eye, since no rotating displacement transducer was used in Galletly's tests. In Table 5 the lowest dimensionless pressure for each of Kirk and Gill's specimens corresponds to first detection of an incipient buckle by the rotating transducer and the subsequent pressures are those at which buckles first became visible to the unaided eye. As can be seen from the first and second value of $10^6\, p/E$ for specimens 4A, 4B, and 4C, a rather large increase in pressure may be required to make the first incipient buckle grow until it is visible. Thus, the meaning of "Buckling Test Results" depends upon the observer.

Notice that Fig. 18 seems at first to contradict Fig. 16. The large buckles measured by the rotating transducer appear to be predominantly inward, whereas those in the photograph appear to be predominantly outward. This is an optical illusion, however. The actual buckles, as seen particularly in the bottom curve in Fig. 18, consist of sharp outward-pointing ridges projecting from relatively gentle valleys. The sharp ridges catch the light and cast definite shadows in the photograph, but if one looks carefully, especially at the middle specimen in Fig. 16, one can see that indeed the ridges do project from gentle valleys.

Comparison of Test and Theory. Table 2 gives the buckling pressures observed by Galletly and by Kirk and Gill and lists the critical pressures obtained with BOSOR5 with use of flow theory and deformation theory. Critical pressures are also given corresponding to use of linear and nonlinear theory with the assumption that the material remains elastic,

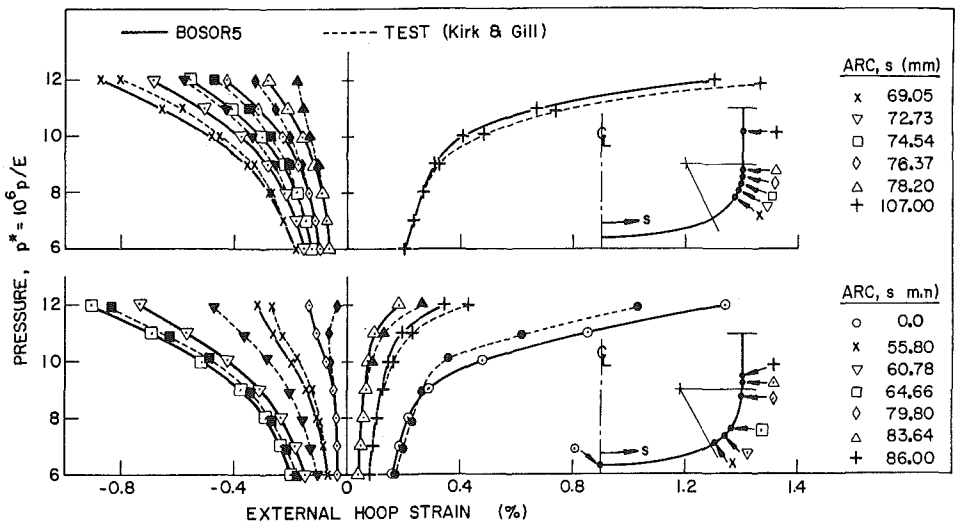

Fig. 11 Comparison of test and theory for the outer fiber hoop strain in specimen 1C, one of the thickest of Kirk and Gill's specimens

The critical pressures predicted by BOSOR5 correspond to incipient nonaxisymmetric harmonic buckling, not to the pressures at which the nonaxisymmetric buckles become visible. These calculated critical pressures represent bifurcation points on the prebuckling load-deflection curves—points at which infinitesimal harmonically varying buckling modal displacements begin to develop. As described in [30] the infinitesimal buckling mode is assumed to have the form

$$\begin{Bmatrix} u \\ v \\ w \end{Bmatrix} = \begin{Bmatrix} u_n(s) \sin n\theta \\ v_n(s) \cos n\theta \\ w_n(s) \sin n\theta \end{Bmatrix} \tag{3}$$

in which u, v, w are the meridional, circumferential, and normal displacement components, s is the distance along the meridian, θ is the circumferential coordinate, and n is the number of waves around the circumference. How these harmonic buckling modes grow with increasing pressure depends on the slope of the postbuckling path and on the manner in which energy is transferred from the essentially membrane axisymmetric prebuckling condition to the postbuckling condition in which considerable circumferential bending is present. The measurements of Kirk and Gill seem to indicate that the postbuckling path has a positive slope initially. The photographs of the buckled specimens (Figs. 16 and 17) indicate that during the postbuckling phase the transfer of energy from membrane to bending occurs only at isolated areas around the circumference, probably causing relief of the circumferential compressive stresses for distances on either side of the buckle which are much longer than the characteristic circumferential wavelength of the buckle itself. However, this description of the postbuckling phenomenon is hypothetical, since BOSOR5 only calculates the buckling eigenvalues and eigenvectors corresponding to harmonic modes of the form (3).

In general BOSOR5 seems to predict buckling at a location nearer to the sphere-torus junction than observed in the tests, and the critical circumferential wave number obtained from the theories in which plasticity is included is somewhat lower than the observed value. For all of the aluminum specimens except 4C the calculated buckling pressures are higher than those observed in the tests, and in the case of specimen 4C theory and test are in reasonably close agreement. A large discrepancy exists between test and theory for the mild steel specimens, however. Possible explanations for this are offered in following sections.

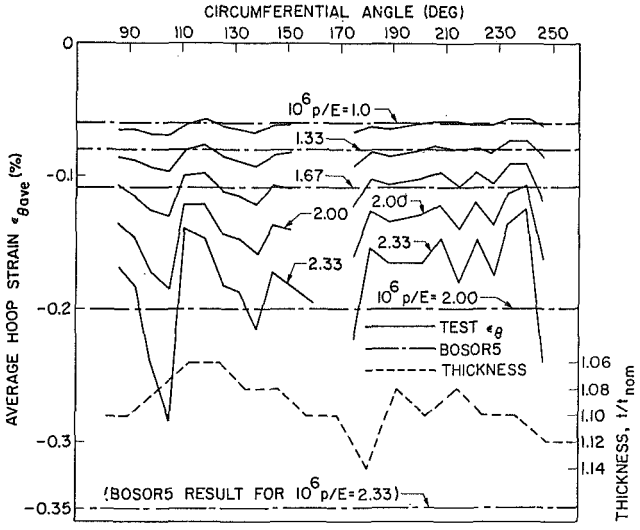

Fig. 12 Average hoop strain distribution measured at latitude z = 13.7 mm in Galletly's mild steel specimen MS3—the latitude z = 13.7 mm (measured from the crown). Corresponds to the maximum in the predicted normal buckling modal displacement.

Predicted State of Stress and Strain at Buckling. Fig. 19 shows approximately how much plastic strain exists at the buckling pressure predicted with use of flow theory for calculation of the constitutive law governing stability. The maximum effective strain always occurs at the inner fiber in the knuckle near the sphere-torus juncture. As seen from Fig. 20, the maximum normal buckling modal displacement is predicted to occur at approximately this location.

Fig. 21 shows the paths in stress space and strain space followed by the material point at which the effective strain is maxi-

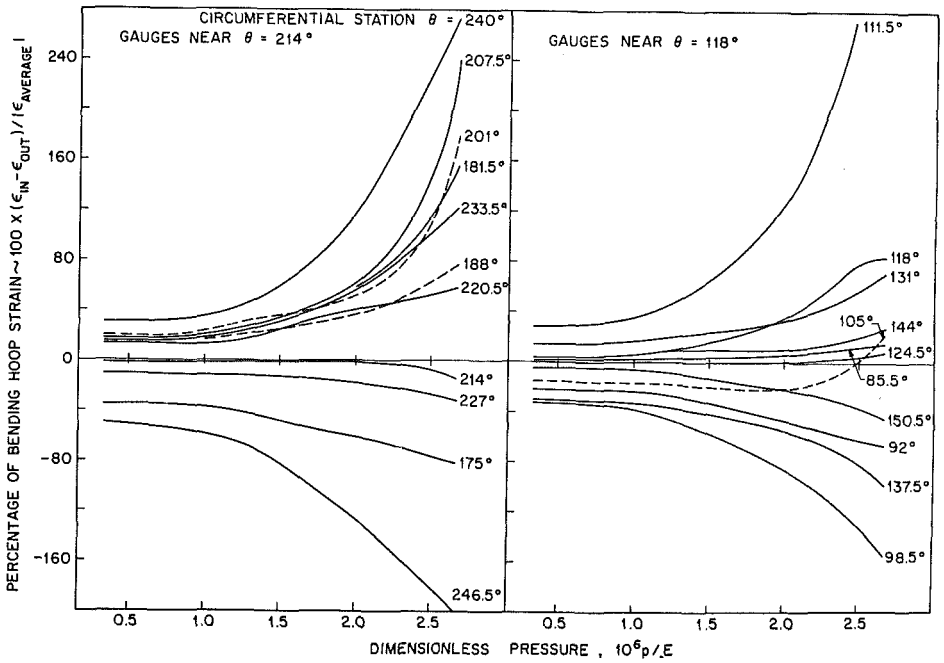

Fig. 13 Growth of circumferential bending strains measured at latitude z = 13.7 mm in Galletly's mild steel specimen MS3

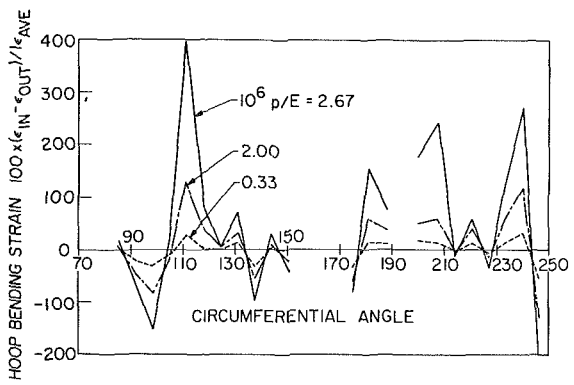

Fig. 14 Circumferential hoop bending strain measured at $z = 13.7$ mm in specimen MS3

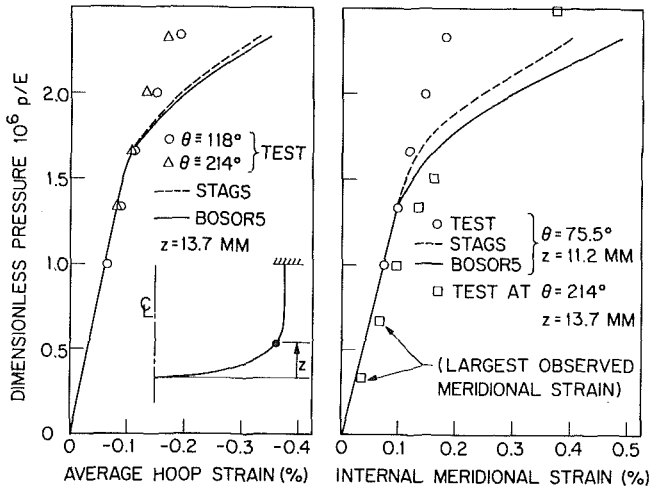

Fig. 15 Comparison of test and theory for hoop and meridional strains in specimen MS3 at latitudes where buckling is predicted to occur

mum. Notice that the loading of the material at this point is not proportional but that the straining of it is approximately proportional. This is partly a consequence of the small degree of strain hardening exhibited by the material used in the tests and partly a consequence of the peculiar mode of deformation of an internally pressurized torispherical head loaded beyond its elastic limit. The curvature of the path in stress space is very sensitive to the degree of strain hardening exhibited by the material. The more strain hardening the more nearly proportional is the loading. Notice that the curves labeled 4A and 4C in the top frame of Fig. 21 do not deviate as dramatically from proportional loading as does the curve corresponding to the mild steel specimen. For strains less than about 1.3 percent the aluminum strain hardens more than does the mild steel. Fig. 16 of [32] also demonstrates the great effect of strain hardening on the path in stress space followed by a material point in a knuckle loaded beyond its elastic limit. Since the concepts of von Mises yield locus, associated flow rule, and isotropic strain hardening—concepts on which the BOSOR5 calculations are based—have been empirically verified only for proportional or near-proportional loading, the discrepancies between theoretical and experimental results in Table 2 may be due partly to inadequacy of this "classical" material model used in BOSOR5.

Flow Theory Versus Deformation Theory. From Table 2 it is seen that the buckling pressures predicted with use of deformation theory are somewhat less than those obtained with use of flow

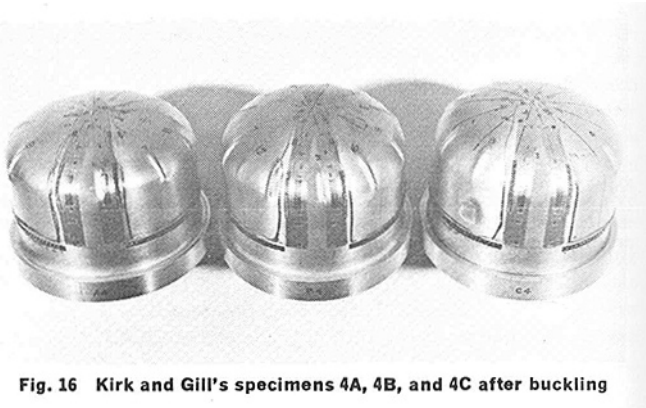

Fig. 16 Kirk and Gill's specimens 4A, 4B, and 4C after buckling

Table 4 Internally pressurized torispherical shells tested by Galletly. Thickness versus axial distance from apex (z) used in the BOSOR5 analysis

	Aluminum Specimens						Mild Steel Specimens							
	$t_n = 0.127$ mm		$t_n = 0.254$ mm		$t_n = 0.254$ mm		$t_n = 0.127$ mm		$t_n = 0.127$ mm		$t_n = 0.127$ mm		$t_n = 0.127$ mm	
	SPEC A1		SPEC A2		SPEC A3		SPEC MS1		SPEC MS2		SPEC MS3		SPEC MS4	
	z (mm)	t/t_n	z (mm)	t/t_n	z (mm)	t/t_n	z (mm)	t/t_n	z (mm)	t/t_n	z (mm)	t/t_n	z (mm)	t/t_n
Segment 1 Spherical	0.0	1.26	0.0	1.04	0.0	1.07	0.0	0.96	0.0	0.92	0.0	1.00	0.0	1.04
	3.30	1.26	3.63	1.04	3.30	1.07	5.08	0.96	1.6	0.92	2.4	1.00	1.93	1.04
	7.87	1.16	8.38	0.97	7.87	1.05			6.35	0.78	7.16	1.14	6.68	1.08
									7.92	0.70				
									9.53	0.70				
Segment 2 Toroidal Knuckle	9.86	1.10	9.86	0.91	9.86	1.05	9.86	1.08	9.86	0.70	9.86	1.14	9.86	0.86
	11.2	1.10	11.6	0.83	14.2	1.07	13.0	1.0	11.1	0.64	13.5	1.06	13.0	0.98
	14.2	1.20	13.1	0.88	19.05	1.03	16.0	7.4	12.7	0.78	18.3	1.06	17.8	1.12
	19.05	1.10	14.7	1.02	22.6	1.00	20.8	1.10	15.1	1.02	23.0	1.10	22.6	1.02
	22.6	1.08	17.1	1.09	29.5	1.09	24.4	1.10	17.5	1.16	28.6	1.08	28.1	1.04
	29.5	1.04	19.5	1.11			31.2	0.94	22.2	1.20				
			24.3	1.08					27.8	1.08				
			29.8	1.03					33.3	1.00				
Segment 3 Cylindrical	35.8	0.76	35.8	1.02	35.8	1.00	35.8	0.72	35.8	1.04	35.8	1.00	35.8	0.88
	42.9	0.96	43.3	0.98	42.9	1.06	44.7	1.08	41.3	1.12	42.1	1.10	41.6	1.10
	52.3	1.14	52.8	1.02	52.3	1.06	54.1	1.08	50.8	1.10	51.6	1.02	51.1	1.08
									69.9	1.12	70.7	1.16	70.2	1.08
	76.4	1.44	76.4	1.02	76.4	1.02	76.4	1.20	76.4	1.12	76.4	1.16	76.4	1.08

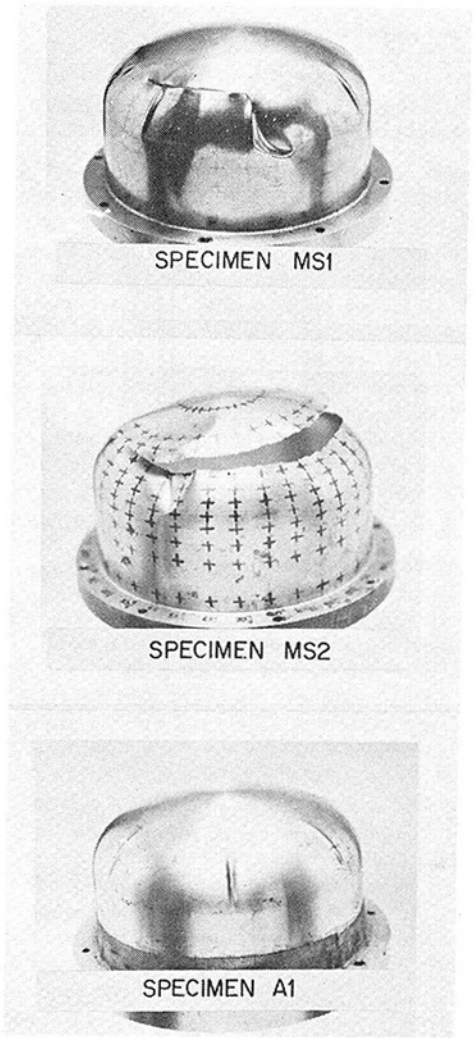

Fig. 17 Galletly's specimens MS1, MS2, and A1 after failure

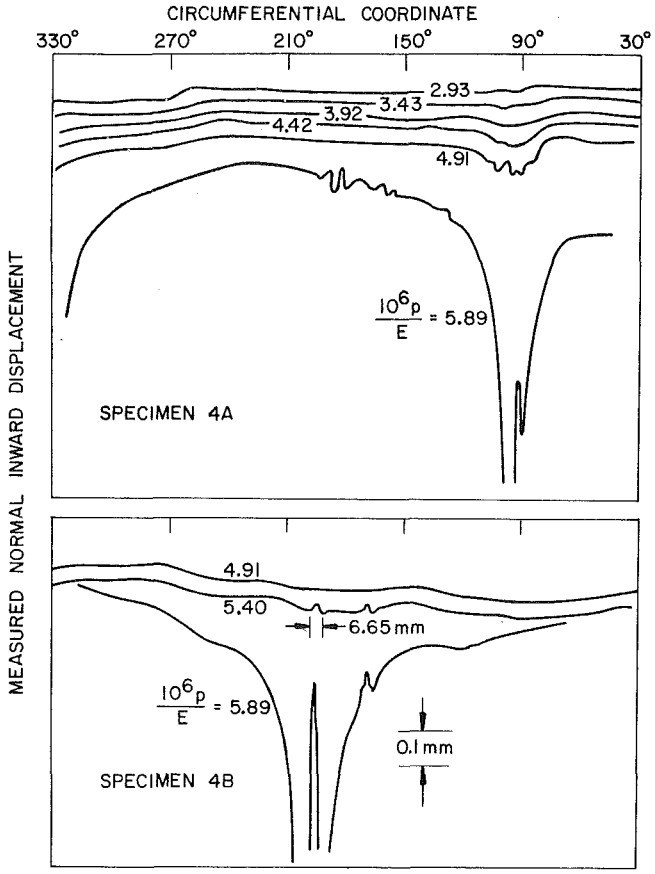

Fig. 18 Incipient buckles and visible buckles measured by Kirk and Gill's rotating displacement transducer

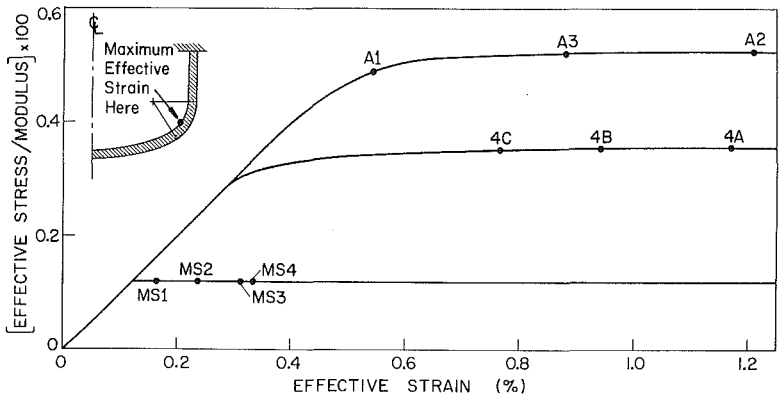

Fig. 19 Maximum effective strain at buckling for Kirk and Gill's and Galletly's specimens

theory. Fig. 22 shows why deformation theory yields lower critical pressures than flow theory. The constitutive equation coefficient C_{55}, which determines the magnitude of the contribution of the change in circumferential curvature during buckling to the change in circumferential buckling moment resultant, is considerably smaller in the region where buckling occurs if deformation theory is used. This coefficient is especially important because the circumferential wavelength of a buckle is small. Therefore, the circumferential bending energy required to form a buckle is perhaps the most significant part of the total strain energy balance associated with buckling.

Fig. 23 shows calculated buckling pressures for specimen MS3 as functions of the number of circumferential waves. The photograph at the top of Fig. 17 indicates that the critical circum-

Table 5 The appearance of buckles with increasing internal pressure

Galletly specimen A1		Kirk and Gill specimens 4A, 4B, and 4C					
Dimensionless pressure $10^6\ p/E$	Circumferential angle of buckle location (deg)	Specimen 4A $10^6\ p/E$	Angle	Specimen 4B $10^6\ p/E$	Angle	Specimen 4C $10^6\ p/E$	Angle
8.25	230	3.44	100	5.39	205	10.81	83
8.64	168	5.40	100	5.89	205	12.29	83
9.13	286	5.90	330	6.39	123	12.29	168
9.71	340	6.39	185	6.89	40	12.29	20
10.49	80	6.87	240	7.37	180	12.78	315
11.26	55	6.87	3	7.37	270	13.28	258
		7.37	110	7.37	325	13.76	129
		7.37	355	7.87	85	15.24	273
		8.36	72	9.34	300	16.71	52
		8.84	146	9.34	8	17.20	196
		8.84	213	10.32	235	17.70	353
		9.82	290	11.79	148		
				12.28	66		

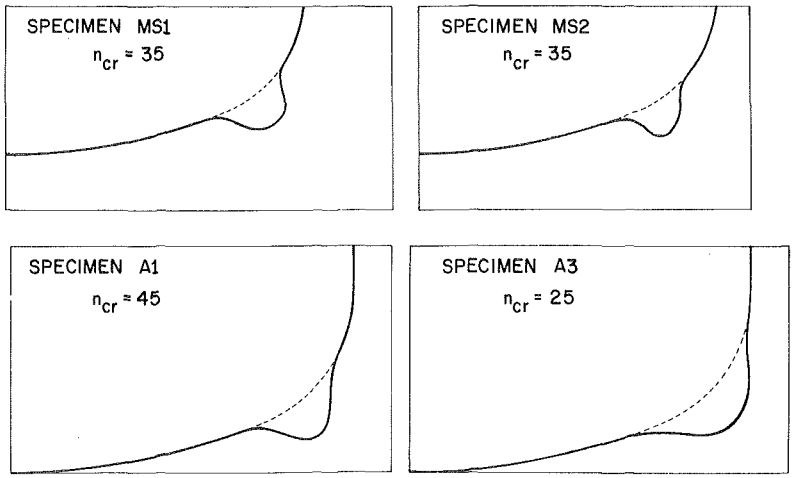

Fig. 20 Predicted buckling modes for four of Galletly's specimens

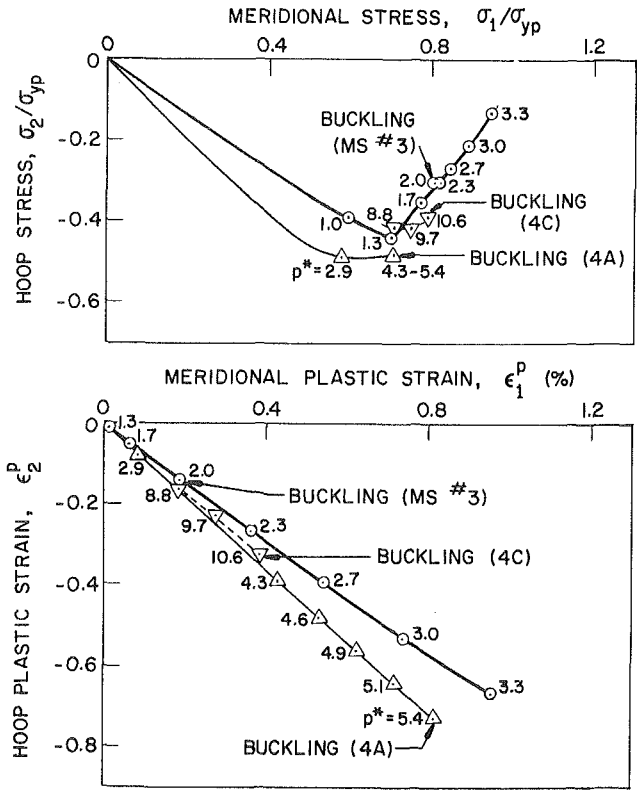

Fig. 21 Predicted paths in stress space and strain space for a point in the toroidal knuckle corresponding to the maximum effective strain

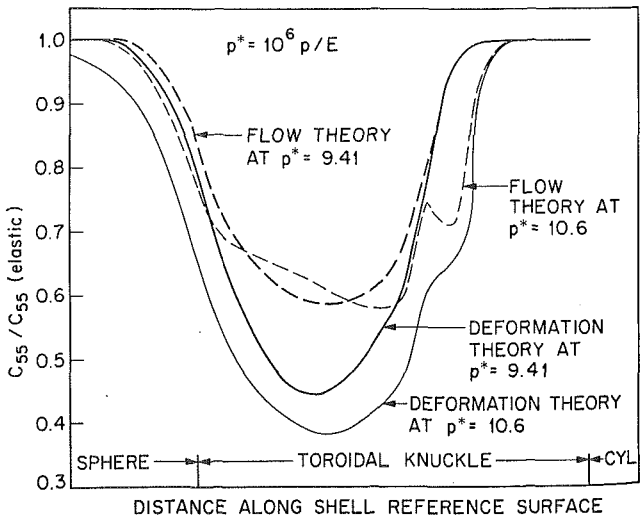

Fig. 22 Predicted reduction of the coefficient for circumferential bending stiffness due to plastic flow in specimen 4C

ferential wave number might be in the range 50–70, whereas the minimum critical pressure obtained by BOSOR5 corresponds to 27 circumferential waves. For n greater than 36 only use of deformation theory leads to a prediction of bifurcation buckling.

Buckling Pressures Predicted With Neglect of Plasticity. The last two columns in Table 2 list the buckling pressures calculated with the assumption that the material remains elastic. Linear (small deflection) theory gives lower critical pressures than does nonlinear theory because the maximum compressive circumferential stress resultant, which causes instability, is greater for linear analysis than for nonlinear analysis. For specimen A3 use of nonlinear theory leads to a prediction that buckling will not occur at all. In this case the peak compressive circumferential stress resultant starts at first to increase with increasing pressure, reaches a maximum value, and then diminishes before the stability determinant vanishes. The critical circumferential wave numbers are higher for the predictions made with neglect of the plasticity than for the predictions with plasticity included.

Discrepancy Between Test and Theory for the Mild Steel Specimens. For the four mild steel specimens the critical pressures observed in the tests are much higher than those calculated by BOSOR5. The material of specimen MS1 was apparently textured, and this might partially explain the very high critical pressure observed with that specimen compared to the critical pressures observed with MS2, MS3, and MS4. Specimens MS1 and MS2 fractured upon buckling. In fact, it is not clear that MS2 buckled at all. From the middle photograph in Fig. 17, it appears that this specimen failed by fracturing along a circumference at a band where the thickness was considerably less than the nominal value. Two buckles, a small one and a large one, are visible on the specimen. Whether or not these were precipitated by fracturing is not known.

The differences in the buckling pressures calculated with BOSOR5 are due to the different nonuniform thickness distributions along the meridian.

It is likely that the buckling modes corresponding to the low critical pressures predicted by BOSOR5 for MS1 through MS4 are not observed in the tests because of initial nonaxisymmetric imperfections in the test specimens. Figs. 12–14 show the growth of nonsymmetric waves at the latitude (z = 13.7 mm) in specimen MS3. This latitude corresponds to the maximum predicted normal buckling modal displacement. Fig. 13 indicates that for dimensionless pressures $10^6\ p/E$ less than about 1.0 these waves grow in proportion to the membrane strain, but that for higher pressures they grow more rapidly. For a dimensionless pressure $10^6\ p/E$ = 2.67, still less than the value 2.73 identified by Galletly as the buckling pressure, the maximum measured difference between inner and outer fiber circumferential strain is four times the membrane strain, as seen from Fig. 14. Since specimen MS3 was machined with greater precision than the other mild steel specimens, MS1, MS2, and MS4, it is likely that similar prebuckling nonaxisymmetric wave patterns developed in them.

Fig. 24 presents schematically a hypothetical explanation for the discrepancy between observed and predicted buckling behavior of the mild steel specimens, in particular specimen MS3. The lowest bifurcation point, $p^* = 10^6\ p/E = 2$, corresponds to buckling with 27 circumferential waves—the mode predicted with BOSOR5. For reasons given in a following paragraph, this mode is assumed to be associated with stable postbuckling growth. That is, the slope of the postbuckling load-deflection curve for $n = 27$ waves is positive. Another bifurcation point exists at $p^* = 3$, this point being associated with a higher number of circumferential waves and an unstable postbuckling load-deflection curve. Such a bifurcation point does not exist if flow theory is used to calculate the stability determinant, but does if deformation theory is used, as seen from Fig. 23. The instability of the postbuckling behavior is postulated because these are

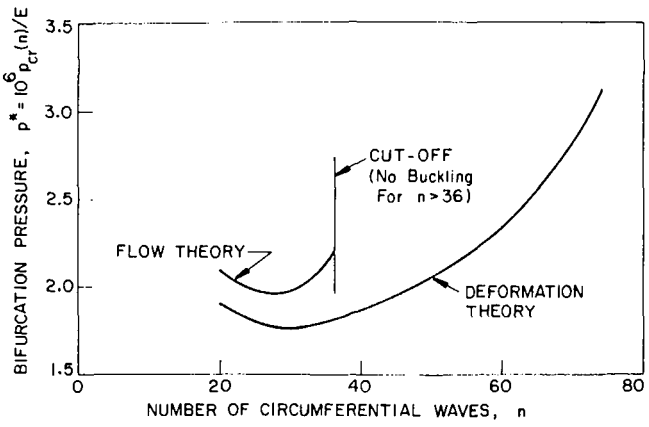

Fig. 23 Predicted bifurcation pressures for Galletly's specimen MS3

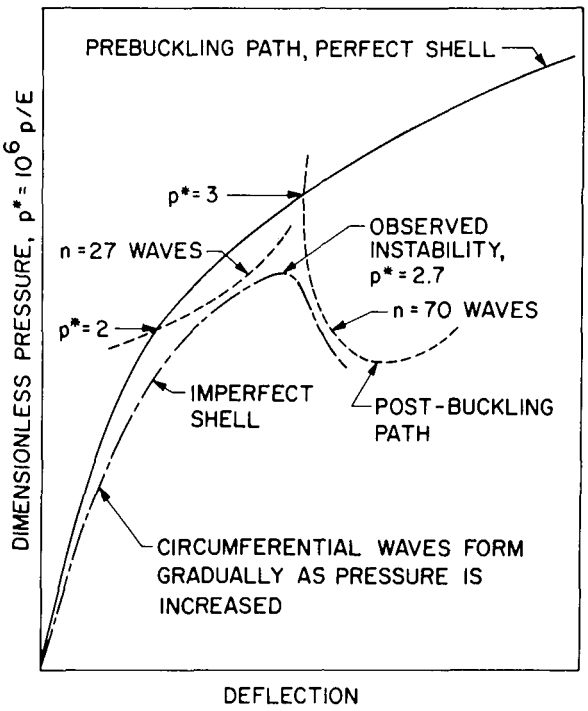

Fig. 24 Hypothesized load deflection curves for perfect and imperfect mild steel specimen MS3 with stable and unstable bifurcation points

the types of buckles observed to appear in the tests accompanied by a snapping noise or by sudden fracture. The actual imperfect shell has a load-deflection curve which reaches a maximum at a pressure for which the first buckle suddenly appears. In the tests, the bifurcation point at $p^* = 2$ and its associated buckling mode are masked by the gradual growth of circumferential waves due to nonaxisymmetric imperfections.

Fig. 25 shows for specimen MS3 the predicted distributions of hoop stress resultants in the toroidal segment for various pressures and the bifurcation buckling mode. Notice that buckling is predicted to occur in the region where the hoop stress resultant is maximum compressive and where the constitutive law coefficients governing stability are reduced because of plastic flow (Fig. 22). As the pressure is increased above the critical value, the peak compressive hoop stress resultant moves away from the sphere-torus juncture and diminishes in value. Fig. 15 of [32] shows that if flow theory is used in the stability analysis the most important constitutive equation coefficient, C_{55}, increases for pressures above the bifurcation point corresponding to $n = 27$ circumferential waves. These two factors—the diminishing of

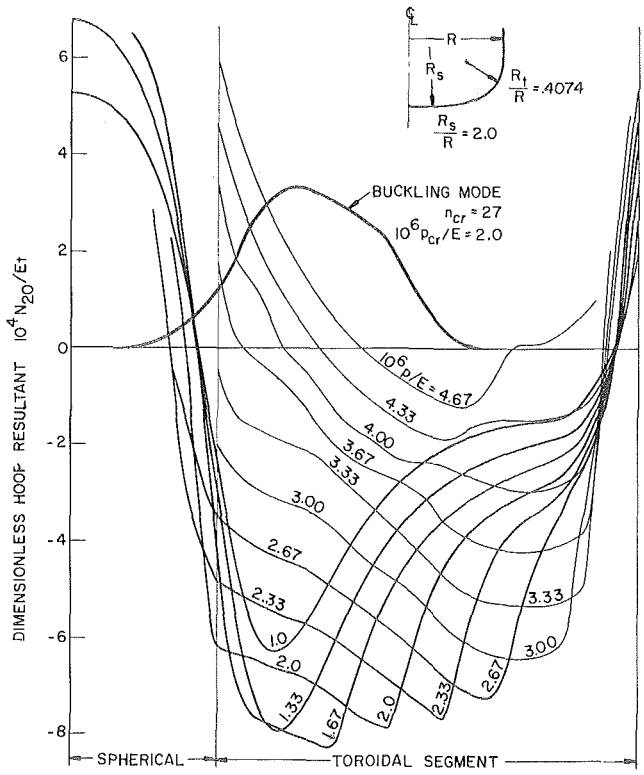

Fig. 25 Predicted buckling mode and hoop stress resultant distributions as functions of pressure for Galletly's mild steel specimen MS3

the peak hoop compression and the increasing of the circumferential bending stiffness—lead to the result shown in Fig. 23 that no bifurcation point exists for $n > 36$ if flow theory is used for the stability analysis. Bifurcation points do exist if deformation theory is used because the constitutive equation coefficients continue to decrease as the effective strain increases. This fact is demonstrated in Fig. 10 of [32].

The buckling mode shown in Fig. 25 probably does not grow much in the postbuckling regime for two reasons. Its appearance causes a circumferentially local decrease in the hoop compression, and further increase in pressure causes the average hoop compression to decrease everywhere around the circumference. For these two reasons the postbuckling curve in Fig. 24 corresponding to 27 waves is drawn with a positive slope.

Conclusions

At the conclusion of this study several questions remain. How much of the discrepancy between test and theory is due to initial nonaxisymmetric imperfections in the specimens and how much is due to inability of the analytical model to predict accurately biaxial flow in situations when the material is loaded nonproportionally? What is an appropriate definition of buckling pressure—when the first incipient buckle forms or when the first buckle becomes visible to the unaided eye? Why do sharp outward-pointing ridges form in plastic buckles whereas only inward buckles seem to form when the material remains elastic? Why does the analysis seem consistently to underestimate the critical circumferential wave number in the buckling mode and overestimate the strains in the knuckle region for pressures above those that cause yielding? How does anisotropy in the material affect the behavior of the heads? What are the characteristics of the postbuckling load-deflection behavior?

Answers to some of these question have been hypothesized, but more work will have to be done to solve completely the problem of nonlinear axisymmetric deformations and bifurcation buckling of internally pressurized elastic-plastic torispherical vessel heads. In particular, an evaluation of classical-type plasticity models for nonproportional loading should be carried out on simple models such as tubes under uniform axial tension and external pressure. The tension and pressure could be varied in such a way as to simulate the nonproportional loading experienced in the knuckle region of an internally pressurized head stressed beyond the proportional limit of its material. In this way the effects of geometrical imperfections and large deflections could virtually be eliminated from the problem, thereby leading to an idea of how much the discrepancy between test and theory is due to use of an inadequate model for nonlinear material behavior. Better analytical models of the material should then be constructed. If possible, ways should be devised for better controlling the circumferential variation of the thickness of specimens for which buckling pressures are being sought. An analytical method should be devised for including nonsymmetric imperfections without the requirement of excessively large amounts of computer time. Finally, it is hoped that more work along similar lines will eventually lead to simple design formulas which account for the possibility of elastic-plastic nonaxisymmetric buckling.

Acknowledgments

The analytical portion of this work was sponsored by the 1975 and 1976 Lockheed Independent Research and Independent Development Programs. The authors are most grateful to Professor S. S. Gill and Mr. Arnold Kirk, who supplied the experimental pressure-strain data, geometrical surveys, and photographs of their specimens. Ernest Esztergar contributed many helpful suggestions which improved the paper considerably.

References

1 Galletly, G. D., "Stress Failure of Large Pressure Vessels —Recommendations Resulting from Studies of the Collapse of a 68 Ft. High × 45 Ft. Dia. Pressure Vessel," Tech Rept. No. 45-57, Shell Development Corp., Emeryville, Calif., Mar. 1957.

2 Galletly, G. D., "Torispherical Shells—A Caution to Designers," TRANS. ASME, Vol. 81, Series B, No. 1, Feb. 1959; also, published in *Pressure Vessel and Piping Design—Collected Papers 1927–1959*, ASME, New York, 1960.

3 Drucker, D. C., and Shield, R. J., "Limit Analysis of Symmetrically Loaded Thin Shells of Revolution," *Journal of Applied Mechanics*, Vol. 26, No. 1, Mar. 1959, pp. 61–68.

4 Shield, R. J., and Drucker, D. C., "Design of Thin-Walled Torispherical and Toriconical Pressure Vessel Heads," *Journal of Applied Mechanics*, Vol. 28, No. 2, June 1961, pp. 292–297.

5 Gerdeen, J. C., and Hutula, D. N., "Plastic Limit Analysis of Hemispherical and Toriconical Head Pressure Vessels," *Welding Research Council Bulletin No. 163*, 1971.

6 Crisp, R. J., and Townley, C. H. A., "The Application of Elastic and Elastic-Plastic Analysis to the Design of Torispherical Heads," *First International Conference on Pressure Vessel Technology*, Delft, 1969, pp. 345–354.

7 Simonen, F. A., and Hunter, D. T., "Elastic-Plastic Deformations in Pressure Vessel Heads," *Welding Research Council Bulletin No. 163*, 1971.

8 Calladine, C. R., "Lower-Bound Analysis of Symmetrically Loaded Shells of Revolution," *First International Conference on Pressure Vessel Technology*, Delft, 1969, pp. 335–344.

9 Save, M., "Verification Experimentale de L'Analyse Limite Plastique des Plaques et des Coques en Acier Doux," Centre de Recherches Scientifiques et Techniques de L'Industrie des Fabrications Metalliques, Brussels, Belgium, Feb. 1966.

10 *Use of Computer in Pressure Vessel Analysis*, ASME, 1969 (Papers and Discussion from ASME Computer Seminar, Dallas, Texas, Sept. 26, 1968).

11 Gerdeen, J. C., "Use of the Computer in the Plastic Limit Analysis of Pressure Vessels," ibid, pp. 37–49.

12 Mescall, J. F., "Large Deflections and Stability of Shells of Revolution," ibid, pp. 1–25.

13 Marcal, P. V., "Elastic-Plastic Analysis of Pressure Vessel Components," ibid, pp. 71–81.

14 Esztergar, E., "Development of Design Rules for Dished Pressure Vessel Heads," *Welding Research Council Bulletin 241*, Apr. 1976.

15 Fino, A., and Schneider, R. W., "Wrinkling of a Large, Thin Code Head Under Internal Pressure," *Welding Research Council Bulletin No. 69*, June 1961.
16 Mescall, J., "Stability of Thin Torispherical Shells Under Uniform Internal Pressure," NASA TN D-1510, *Collected Papers on Instability of Shell Structures*, Dec. 1962, pp. 671–692.
17 Adachi, J., and Benicek, M., "Buckling of Torispherical Shells Under Internal Pressure," *Experimental Mechanics*, Vol. 4, No. 8, Aug. 1964, pp. 217–222.
18 Thurston, G., and Holston, A. A., Jr., "Buckling of Cylindrical Shell End Closures by Internal Pressure," NASA CR-540, July 1966.
19 Bushnell, D., "Stress, Stability and Vibration of Complex, Branched Shells of Revolution," *Computers & Structures*, Vol. 4, 1974, pp. 399–435.
20 Cohen, G. A., "Computer Analysis of Ring-Stiffened Shells of Revolution," NASA CR 2085, Sept. 1972.
21 Anderson, M., Fulton, R., Heard, W., and Walz, J., "Stress, Buckling and Vibrations Analysis of Shells of Revolution," *Computers & Structures*, Vol. 1, 1971, pp. 157–192.
22 Svalbonas, V., and Key, J., "Static, Stability and Dynamic Analysis of Shells of Revolution by Numerical Integration—A Comparison," *Nuclear Engineering and Design*, Vol. 27, 1974, pp. 30–45.
23 Kalnins, A., "Analysis of Shells of Revolution Subjected to Symmetrical and Nonsymmetrical Loads," *Journal of Applied Mechanics*, Vol. 31, 1964, pp. 467–476.
24 Brown, K. W., and Kraus, H., "Stability of Internally Pressurized Vessels with Ellipsoidal Heads," presented at 2nd National Congress on Pressure Vessels and Piping Technology, San Francisco, June 23–27, 1975.
25 Bushnell, D., and Galletly, G. D., "Comparisons of Test and Theory for Non-Symmetric Elastic-Plastic Buckling of Shells of Revolution," *International Journal of Solids Structures*, Vol. 10, 1974, pp. 1271–1286.
26 Kirk, A., and Gill, S. S., "The Failure of Torispherical Ends of Pressure Vessels Due to Instability and Plastic Deformation—An Experimental Investigation," *International Journal of Mechanical Science*, Vol. 17, 1975, pp. 525–544.
27 Galletly, G. D., "Internal Pressure Buckling of Very Thin Torispherical Shells—A Comparison of Experiment and Theory," Paper G2/3, 3rd International SMiRT Conference, London, Sept. 1975.
28 Bushnell, D., "BOSOR5-Program for Buckling of Elastic-Plastic Complex Shells of Revolution Including Large Deflections and Creep," to appear in *Computers & Structures*, 1976.
29 Bushnell, D., "Large Deflection Elastic-Plastic Creep Analysis of Axisymmetric Shells," *Numerical Solution of Nonlinear Structural Problems*, AMD-Vol. 6, R. Hartung, ed., ASME, New York, 1973, pp. 103–138.
30 Bushnell, D., "Bifurcation Buckling of Shells of Revolution Including Large Deflections, Plasticity and Creep," *International Journal of Solids Structures*, Vol. 10, 1974, pp. 1287–1305.
31 Bushnell, D., "Buckling of Elastic-Plastic Shells of Revolution with Discrete Elastic-Plastic Ring Stiffeners," *International Journal of Solids Structures*, Vol. 12, 1976, pp. 51–66.
32 Bushnell, D., "Nonsymmetric Buckling of Internally Pressurized Ellipsoidal and Torispherical Elastic-Plastic Pressure Vessel Heads," ASME Paper No. 76-PVP-25, presented at ASME Petroelum Mechanical Engineering and Pressure Vessels and Piping Conference, Mexico City, Sept. 19–24, 1976.
33 Almroth, B. O., Brogan, F. A., and Stanley, G. M., "Structural Analysis of General Shells, Vol. III, User Instructions for STAGS C," LMSC-D502277, Lockheed Missiles and Space Company, Palo Alto, Calif., Dec. 1975.